RSC Advances

Graphical Abstract

The increase in oxygen functionalities on GO with increasing use of oxidizing agent, results in (i) amplification of redox pseudocapacitive current and (ii) improves metal ion adsorption.

Impact of the Degree of Functionalization of Graphene oxide on the Electrochemical Charge Storage Property and Metal ion Adsorption

Mahesh M. Kadam, Omkar R. Lokare, Kota V.M.K. Kireeti, Vilas G. Gaikar and Neetu Jha[*]

[1]Department of Chemical Engineering,

Institute of Chemical Technology,

Mumbai - 400019

Corresponding author : Tel.: +91-022-33612013;

Fax: +91-022-33612020;

e-mail: nr.jha@ictmumbai.edu.in

1   **Abstract**

2   Graphene oxide (GO) samples were prepared at room temperature using modified Hummer's

3   method. The quantitative variation of oxidizing agent for the oxidation of graphene sheets

4   resulted in increasing the oxygen functionalities on GO samples. The Qualitative analysis of

5   functional groups and surface charge variation was studied using Fourier transform infra-red

6   (FTIR) spectroscopy and zeta potential respectively. Different oxidation degrees of GO was

7   investigated by X- ray diffraction (XRD), Raman and X-ray photoelectron spectroscopy (XPS).

8   The electrochemical charge storage property of the GO samples were studied using   two

9   electrode supercapacitor cell. The fabricated supercapacitor demonstrates linear enhancement in

10   the specific charge storage with an increase in the oxidation of GO samples. Maximum charge

11   storage of 71 F/g has been obtained with highly oxidized GO sample at room temperature. The

12   adsorption of metal ions from the aqueous solution has also been studied with the variation in the

13   degree of functionalization of the GO samples. It was observed that increasing oxygen

14   functionalities from GO-1 to GO-5 amplifies the uptake of metal ions [Cd(II) and Cu(II)]. The

15   experimental data fits well in Langmuir adsorption model, indicating monolayer adsorption of

16   metal ion on GO samples.

17   *Keywords: Graphene Oxide, Charge storage, Supercapacitor, Cyclic Voltammetry, Adsorption.*

18

1. Introduction

Graphene has attracted great interest worldwide for its excellent mechanical, electrical, thermal and optical properties. The remarkable properties of graphene reported so far include high value of Young's modulus (~1100 GPa), fracture strength (125 GPa), thermal conductivity (~5000 W/m/K) and specific surface area (2630 m^2/g).[1] Many techniques have been developed recently for the production of graphene, such as micro-mechanical exfoliation of highly ordered pyrolytic graphite, epitaxial growth, chemical vapor deposition and the reduction of graphene oxide(GO).[2] GO is an atomic sheet of graphite containing several oxygenated functional groups on its basal planes and edges, owing to the mixing of sp^2 and sp^3 hybridized carbon atoms.[3] GO has many applications in various fields such as photocatalysts, memory devices, energy storage and drug delivery agents.[4-7] The two amazing characteristics of GO is that; firstly, it can be produced using inexpensive graphite as raw material by cost-effective chemical methods in high yields, and secondly, it is highly hydrophilic and forms stable aqueous colloids which facilitate the assembly of macroscopic structures. Both these properties are important for large-scale use of graphene oxide.

Three major methods have been used for the synthesis of GO. Pioneering work in this area was done by Brodie for ascertaining carbon atomic weight of graphite.[8] Later Hummer[9] and Staudenmaier[10] developed popular methods with improved experimental safety and reduced formation of toxic gases. Since then, oxidation of graphite has not been paid much attention until recently, when GO was realized as a promising potential route for the large scale production of graphene.[11] There are few reports in the literature focusing on optimizing the degree to which graphite should be oxidized for its efficient exfoliation to single layers of GO.[12] The oxidation mechanism of GO and their structures are still indefinable due to its nonstoichiometry and strong hygroscopic nature. Szabo et al., studied in detail the evolution of surface functional groups in a

1 series of progressively oxidized GO by the Brodie method.[13] The model proposed that GO,

2 exhibited a carbon network comprising of two regions: *trans*-linked cyclohexane chairs and

3 ribbons of flat hexagons with C=C double bonds decorated with functional groups.[13] The

4 aromatic structure of graphite was completely destroyed by the oxidation using Brodie method.

5 Therefore, Hummers method has been found to be more apposite for preparing GO. Lerf et al,

6 had proposed a model for GO consisting of two kinds of regions: aromatic regions with

7 unoxidized benzene rings and regions with aliphatic six-membered rings.[14] The comparative area

8 of the two regions depends on the degree of oxidation, with hydroxyl and epoxy groups located

9 on the interior of GO and carboxyl (COOH) groups at the edges of sheets.[14] Wilson et al.[15] found

10 that the latter model was consistent with their experimental observations. However, the influence

11 of layer spacing on the exfoliation of GO sheets was not discussed in their report. It is known

12 that the functional groups and heteroatoms on the carbon sheets improve the wettability of GO

13 electrode due to increased number of hydrophilic polar sites and thus enhance the over-all charge

14 storage capacitance of the electrodes.[16] Graphite and graphene possess sp^2 hybrid carbon atoms

15 which are partially degraded to sp^2–sp^3 hybrid atoms in GO. Because of the lesser π–π stacking

16 stability and poor conductivity, GO was theoretically claimed to be inappropriate electrode

17 material for supercapacitors.[17] However, Xu et al.[18] reported that the GO, which is an

18 intermediate during graphene synthesis, exhibits higher capacitance than graphene due to an

19 additional *pseudo*-capacitance effect of the attached oxygen-containing functional groups on its

20 basal planes. Taking into consideration its lower cost and shorter processing time, GO may

21 become a better choice than graphene as the electrode material for supercapacitors.[18] Further, the

22 presence of the negative charged oxygenated functional groups and the aromatic network

23 influences the adsorptive behavior of GO.[19] It is also known as a potential adsorbent for the

24 removal of organics such as methylene blue, methyl violet, orange G, malchite green, methyl

1. green, acridine, phenols[19-22] and inorganic contaminants viz; Zn(II), Cu(II), Cd(II), Pb(II), Co(II),

2. Eu(III), U(IV), Au(III), Pd(II), Pt(IV) etc. from aqueous solutions.[23-28]

3. In the present study, we have focused on introducing varying scale of oxygenated functional

4. groups on the GO surface. We used the modified Hummers method to synthesize GO at 300 K.[31]

5. Different degrees of oxidation of graphite were achieved by altering the dosage of oxidizing

6. agent ($KMnO_4$) during the synthesis. In total, five GO samples were synthesized and labeled as

7. GO-1, GO-2, GO-3, GO-4 and GO-5, respectively in the order of increasing the level of

8. oxidation. All the samples were characterized in detail for degree of oxidation, surface

9. properties, interlayer spacing and zeta potential. The effect of degree of oxidation on the charge

10. storage property of GO was evaluated using electrochemical two electrode cyclic voltammetric

11. and galvanostatic charge-discharge method.

12. As Cu and Cd are few of the major pollutants in the marine and waste stream coming from

13. mining operations, textile, electrochemical, and petrochemical industries.[29].These non-

14. biodegradable, persistence pollutant effects the water bodies and accumulate in the

15. environmental elements *viz.* food cycle, which may significantly endanger human health.[29,30]

16. Hence, adsorption extent of metal ions, Cu(II) and Cd(II) on GO (1-5) samples at different pH (2

17. and 4) were also studied in detail using GO samples.

18. **2. Materials and Characterization**

19. *2.1 Materials*

20. Potassium permanganate ($KMnO_4$) (99%), cadmium chloride ($CdCl_2$) (99%) and copper chloride

21. ($CuCl_2$) (99%) were used as received from Sigma Aldrich Pvt. Ltd., Mumbai. Graphite powder

22. of 99% purity and standard solution of cadmium and copper for ICP-AES was obtained from

23. Alfa Aesar Pvt. Ltd. Sulfuric acid (H_2SO_4) (98%) and hydrochloric acid (36%)were obtained

1   from S.D. Fine Chemicals. De-ionized (DI) water obtained from Millipore, was used for all the

2   experiments.

3   *2.2 Characterization*

4   FTIR spectra of the GO samples were carried out using Bruker-VERTEX 80v FTIR

5   spectrophotometer in transmittance mode with 128 scan using the KBr pellet method with

6   resolution of 1 cm^{-1}. XRD spectra of the samples were recorded in a wide angle range (2θ =5° to

7   80°) on D8-Adavance Bruker X- ray Diffractometer, with scanning speed of 0.016 sec/step,

8   using monochromatized CuK$_{\alpha}$ radiation of wavelength 1.54 Å. Malvern zetasizer nano ZS90 was

9   used to measure the zeta potential of the GO samples. The Raman spectra of GO sample were

10 recorded in the range 1000 to 4000 cm^{-1} at an ambient temperature (303K) with a Horiba HR 800

11 model equipped with laser excitation wavelength 514.5 nm, spot size 1μm and incident power

12 ~10mW. X-ray photoelectron spectroscopy (XPS) of GO sample were carried out on AXIS

13 ULTRA, AXIS 165, equipped with integrates the Kratos patented magnetic immersion lens,

14 charge neutralisation system with new spherical mirror analyser and Al Kα X-rays as the source

15 (hυ = 1486.6 eV). The electrochemical impedance measurements for GO samples were measured

16 at normal temperature and pressure (NTP) conditions on LCR (Wayne Kerr 6500B, Chichester,

17 West Sussex, UK) within the frequency range of 20 Hz to 20MHz and bias potential of 1V.

18 *2.3 Inductive Coupled Plasma- Atomic emission spectroscopy (ICP-AES)*

19 Metal ion (Cd(II) and Cu(II)) concentrations, before and after adsorption were analyzed by ICP-

20 AES Arcos M/s. Spectro, Germany. The working parameters of charge coupled device (CCD)

21 and the radio frequency generator maximum were 1.6 KW, 27.12 MHz. For injection of samples

22 into the plasma, the pump speed was maintained at 30 rpm. The flow rate of argon was

1   maintained at 1, 0.8, and 12 $dm^3.min^{-1}$ for auxiliary gas, the nebulizer gas, and plasma generation

2   respectively.

3   **3. Experimental Details**

4   *3.1. Synthesis of graphene oxide*

5   The suspension of exfoliated graphite (Ex-G) (200 mg) particles were prepared in conc. H_2SO_4

6   (100 cm^3), followed by the slow addition of oxidizing agent ($KMnO_4$) and kept for 3hr under

7   continuous stirring. [31] The reaction mixture was diluted with 100 cm^3 DI water and subsequently

8   stirred for 24 hr. The reaction mass was further treated with 600 cm^3 of water, followed by

9   addition of 30% H_2O_2 solution (20 cm^3), which acts as the bleaching agent. The resulting

10   mixture was then centrifuged and the solid residue obtained was sonicated in 7N HCl (100 cm^3)

11   for the removal of MnO_2 impurities. The GO thus obtained was washed thoroughly with DI

12   water till neutral pH was obtained. The samples prepared were labelled as GO-1, GO-2, GO-3,

13   GO-4 and GO-5 corresponding to the quantitative variation of $KMnO_4$ dosage as 0.2, 0.6, 1.0,

14   1.4 and 1.8 g, respectively. GO suspensions obtained in DI water has been pictorially shown in

15   Fig. S1 of ESI.

16   *3.2 Electrode fabrication and electrochemical measurements*

17   The aqueous GO suspension was prepared by sonicating the sample for 30 mins. The electrode

18   for capacitor was prepared by dropcasting the GO suspension on 1 cm (diameter) circular

19   graphitized carbon paper followed drying at 303K for 24 h and further use in Teflon swagelok

20   cell with stainless steel current collector.[32] The swagelok cell comprise of two electrodes that are

21   isolated from electrical contact by a porous separator soaked in 0.5M H_2SO_4. The

22   electrochemical performance was examined on multichannel potentiostat and galvanostat using

23   Metrohm, µAutolab type III electrochemical workstation. The cyclic voltammetry was carried

1   out at the scan rate of 30 mV/s and galvanostatic charge / discharge at 1A/g (current density) at

2   an operating voltage window of 0 - 0.8V.[33]

3   *3.3 Metal ion Adsorption from aqueous solutions*

4   The batch adsorption equilibrium uptake of divalent Cu and Cd ions on GO was determined at

5   pH 2 and pH 4. The GO samples (4 mg) were ultrasonicated in 10 cm^3 of DI water and then

6   mixed with 10 cm^3 of metal ion solution. The pH of solution was adjusted by the addition of

7   0.1M HCl and NaOH. The suspension was equilibrated for 24 h at 303 K. After equilibration, the

8   GO particles were separated by centrifugation. The amount of metal ions adsorbed on GO was

9   estimated from eq (1)[19, 23]

10     $q_e = \dfrac{(C_0 - C_e)V}{m}$ (1)

11   where, C_0 (mg.dm^{-3}) is initial metal ion concentration in aqueous solution and the C_e (mg.dm^{-3}) is

12   equilibrium liquid phase metal ion concentration, *V* is the volume of the suspension, and *m* is the

13   mass of GO used for the adsorption. For the isotherm studies, the metal ion (Cd and Cu) were

14   varied from 10 to 200 mg dm^{-3} at pH = 4 as both the metal ions exist as divalent positive ions at

15   this pH.[19,23]

16   **4. Results and Discussion**

17   **4.1. X-ray diffraction analysis**

18   The XRD patterns provide information on the contents of oxidized GO part and non-

19   oxidized graphite part in the sample.[19] The XRD spectra (Fig. 1) of the synthesized GO samples

20   shows significant change in the crystallinity of GO at different degrees of oxidation. The starting

21   material graphite shows a highly intense peak at 26° corresponding to (002) reflection from

22   hexagonal carbon structure. The sample GO-1 shows two peaks which is characteristic of the

23   ordered (002) hexagonal graphitic planes (2θ = 26°) and (001) reflections at 2θ=11.10°

1 corresponding to defected hexagonal graphitic structure due to the insertion of oxygenated

2 functional group on the oxidized graphitic surface.[19,34-40] Further, with an increase in oxidation

3 from GO-2 to GO-5 the peak at 26° disappears and simultaneously we get a single peak in the

4 range of 10-12°. This reveals that large number of oxygen-containing groups have been

5 introduced on GO sheet.[19] The addition of oxygenated functional groups (-OH, C-O-C, C=O) on

6 graphite lattice, shifts (001) reflections to lower 2θ value of 11.10, 11.0, 10.82, 10.52 and 10.34

7 for the samples GO-1 to GO-5 compared to 26° for graphite. This also increases the interlayer

8 spacing (Bragg's equation) of graphite sheets from 0.34 nm in case of graphite to 0.79, 0.8, 0.82,

9 0.84 and 0.85 for GO-1, GO-2, GO-3, GO-4 and GO-5 samples, respectively (Fig. S2, ESI†).

10 The interlayer spacing of all GO samples is more than ~2.4 times higher than pristine graphite

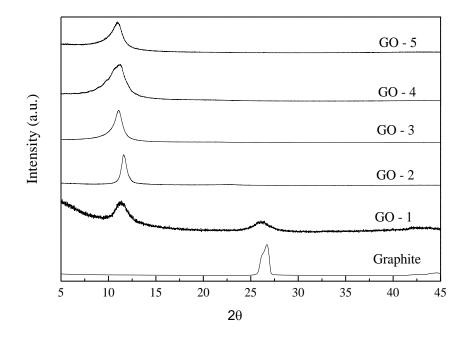11 (0.34 nm), which is well in agreement with reported literature.[19]
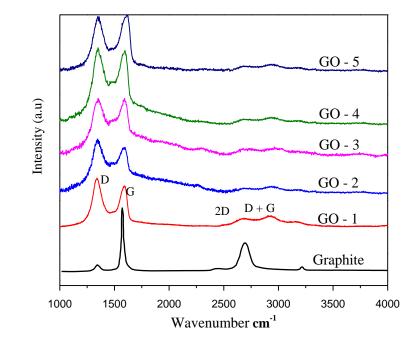

Fig. 1: XRD patterns of GO samples

12

1 **4.2. Raman spectroscopy analysis**

2 Raman spectra (Figure 2) of all GO samples shows two characteristic peaks *viz*. (D

3 band)~1340 cm^{-1} and (G band)~1590. It is known that the G band indicates the first-order

4 scattering of the E_{2g} mode related to sp^2 hybridized C atoms while the D band designates the A_{1g}

5 symmetry mode signifying the generation of defects in the graphite material (such as bond-angle

6 and bond-length distortions, vacancies, edges etc) due to the conversion of sp^2 -hybridized

7 carbon to sp^3-hybridized carbon.[19,40] Oxidation of graphite in GO-1 leads to the G band shift

8 towards higher wavenumber (1592 cm^{-1}) while the D band has a higher intensity, which can

9 attributed to the formation of defects and disorder such as the presence of in-plane hetero-atoms,

10 grain boundaries, aliphatic chain, etc. As the oxidation increases, the G band shifts towards a

11 higher wavenumber, the maximum shift of 1599 cm^{-1} was observed for the highest oxidation

12 level, GO-5 sample. This shift in G band is related to the formation of new sp^3 C centers in the

13 graphite lattice.[40] The full width half maxima (FWHM) of the G band with increasing oxidation

14 level was obtained as 75, 92, 131, 136, and 142 cm^{-1}, for the samples GO-1, GO-2, GO-3, GO-4

15 and GO -5, respectively. Similarly, the intensity of D band also gets affected with the varying

16 oxidation level in all GO samples. The D band intensity increases with increasing oxidation for

17 (GO-1 to GO-3) while it becomes constant at higher oxidation level (GO-4 and GO-5). The

18 FWHM of the D band linearly increase with increase in the oxidation levels representing that the

19 oxidation process influences the in-plane sp^2 domains of the graphite with defects.[40,41] The

20 intensity ratio of I_D/I_G bands is inversely relative to average aromatic cluster size in GO.[19] Fig.

21 S3 of ESI† shows non monotonous pattern of I_D/I_G ratio for the five samples, it increases for

22 GO-1 and GO-2 (lower oxidation levels) and then decreases followed by saturation for higher

23 level oxidized samples. The average aromatic cluster size was calculated by using eqn. 2.[40,42]

10

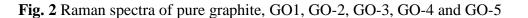1 $$L_a = [(2.4 \times 10^{-10})(\lambda)]/(I_D/I_G)$$ (2)

2   where, L_a is the average crystallite size of the sp^2 domains, λ is the input laser energy, I_D and I_G

3   are the intensity of the D and G bands, respectively. The L_a value of the precursor graphite was

4   calculated to be 124.5 nm while for samples GO-1, GO-2, GO-3, GO-4 and GO-5, the calculated

5   values are 16.14, 13.45, 14.13, 15.25, 15.85 nm, respectively. These results indicate that the

6   average crystallite size decreases with oxidation, resulting in breaking of crystallites and the

7   formation of defects, disorders, sp^3 hybridization and changes in crystallinity. Further, L_a starts

8   increasing for GO-3 sample and becomes almost constant (GO-4 and GO-5) at higher levels of

9   oxidation. The decrease in I_D/I_G ratio and increase in the L_a values at higher oxidation levels is

10   compensated by the increase in the FWHM of the G band.[40] The above results are in well

11   agreement with the previous investigations on the crystallite size of GO for different degrees of

12   oxidation.[40,43]

13   Another significant feature in the Raman spectra of graphite is the presence of 2D (an

14   overtone of the D band) and D + G band at ~2680 cm^{-1} and ~2945 cm^{-1}, respectively.[35,43] The 2D

15   band is very sensitive to the stacking order of the graphite along the c-axis and hence is used to

16   evaluate the structural parameters of the c-axis orientation.[42] The intensity of the 2D and D + G

17   band is smaller and broadens after oxidation. Decrease in the 2D band intensity is attributed to

18   the breaking of the stacking order due to the harsh chemical oxidation reactions which results in

19   the formation of different types of oxygenated functional groups at the basal plane and also at the

20   edges.

1

2   **Fig. 2** Raman spectra of pure graphite, GO1, GO-2, GO-3, GO-4 and GO-5

3 **4.3. X-ray photoelectron spectroscopic(XPS) analysis**

4   XPS provides clear evidence of percentage and type of functional group attached to GO

5 sheets (Fig. 3). The C1s peaks of the XPS spectra shows the main peak at 284.0 and 284.5 eV

6 corresponding to the graphitic carbon, and other peak at 285.5 eV, 286.5 eV, 287.5 and 288.4 eV

7 corresponding to C-O, C-O-C, C=O bonds in carbonyl and O–C=O in carboxylic and/or ester

8 groups respectively.[19,44] The consecutive increase in the intensity of epoxide (O–C–O) groups

9 form GO-1<GO-2<GO-3<GO-4<GO-5 as compared to O–C=O and C-O was observed. The GO-

10 5 shows ~5 times higher amount of epoxy group as compare to GO-1. As the oxidation level is

11 increased, total intensity of non-aromatic carbon increases with the corresponding lowering of

12 aromatic carbon intensity. This above trends is in agreement with earlier report in GO by

13 Krishnamoorthy *et al.*[40]

1   The integrated intensity of aromatic ($I_{aromatic\ carbon}$) and non-aromatic ($I_{non-aromatic\ carbon}$)
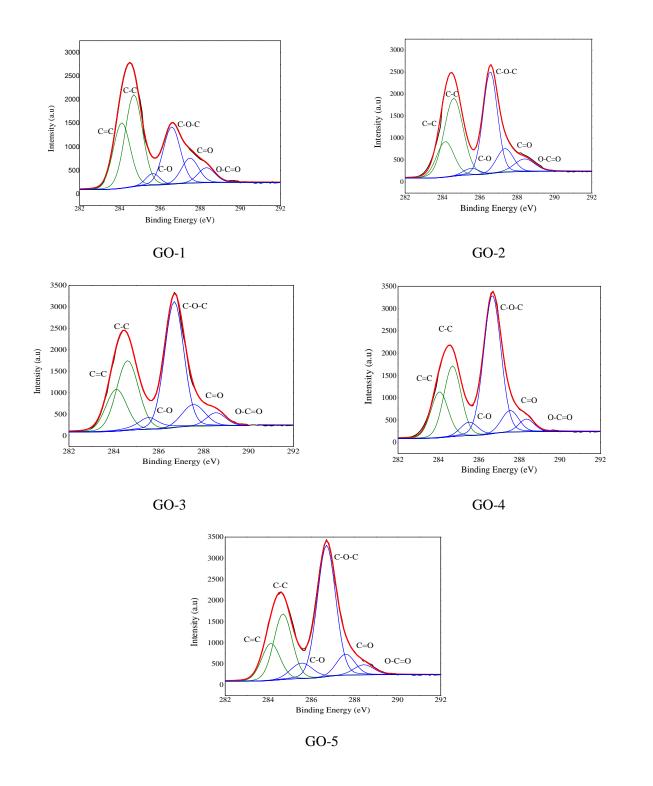
2   carbon obtained from C1S XPS spectra and the integrated intensity of GO (I_{GO}) and graphite

3   ($I_{Grapite}$) obtained from XRD spectra was further employed to calculate oxidation degree of the

4   GO series by using eqn. 3. [19]

5    $Degree\ of\ Oxidation\ (\%) = \dfrac{I_{non-aromatic\ carbon}}{I_{non-aromatic\ carbon}+I_{aromatic\ carbon}} \times \dfrac{I_{GO}}{I_{GO}+I_{Grapite}} \times 100\%$

6   (3)

7   The degree of oxidation (21%, 52%, 58%, 62%, and 64% was calculated for GO-1, GO-

8   2, GO-3, GO-4 and GO-5 samples respectively. It confirms increases in the degree of oxidation

9   from GO-1 to GO-5. Yan *et al.*[19] reported successive increment in degree of oxidation with
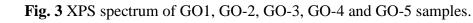
10   increase in oxidant amount with maximum 58% of oxidation degree of GO. The Raman, XRD

11   and XPS pattern confirms that increase in the oxidant dosage increases the degree of oxidation.

12

13

GO-1

GO-2

GO-3

GO-4

GO-5

1

2   **Fig. 3** XPS spectrum of GO1, GO-2, GO-3, GO-4 and GO-5 samples.
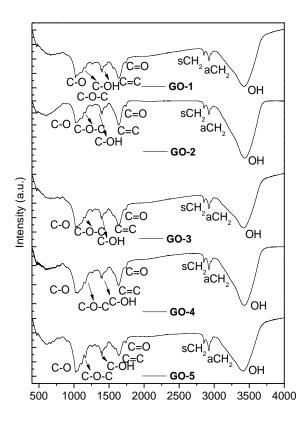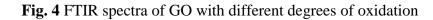
3

4

1   **4.4 FTIR spectroscopic analysis**

2   The FTIR spectra of the GO samples are shown in Fig. 4. The spectra show a band at

3   1573 cm^{-1} due to the presence of C–C stretching in the graphitic structure. The peak at 3416 cm^{-1}

4   is attributed to the O-H stretching vibrations, which appears due to the presence of moisture or

5   adsorbed water. The band at 1728 cm^{-1} corresponds to the stretching vibrations from C=O, 1620

6   cm[-1] to skeletal vibrations from unoxidized graphitic domains and hydroxyl groups at GO, 1420

7   cm[-1] corresponds to OH deformation peak, 1220 cm^{-1} corresponding to C-O stretching vibrations

8   and 1052 cm^{-1} is attributed to C-O stretching vibrations.[40,44] The presence of these peaks

9   confirms the synthesis of functionalized graphene oxide sheets.[40] The polar oxygen functional

10   group renders hydrophilic character to GO and hence it can be easily dispersed in the polar

11   solvents.

12

13   **Fig. 4** FTIR spectra of GO with different degrees of oxidation
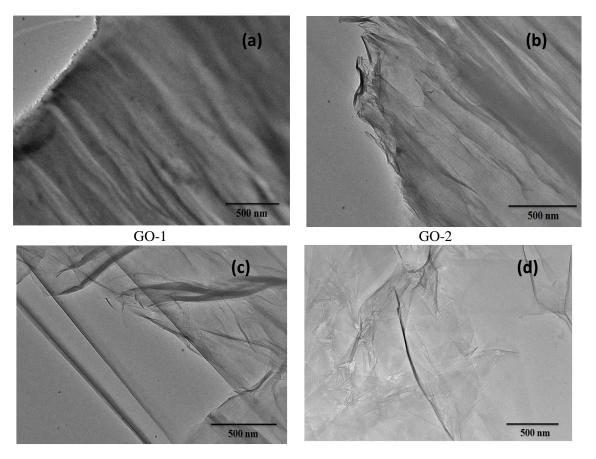
15

4.5. Zeta Potential

The zeta potential is a physical property exhibited by the particles in dispersion and is a vital parameter for characterizing the electrical properties of interfacial layers in dispersion. The zeta potential values of GO-1, GO-2, GO-3, GO-4 and GO-5 were measured to be -40, -43, -54, -58 and -61 mV respectively (Fig. S4, ESI†). The successive increment in the degree of oxidation, increases negatively charge oxygenated functional groups that are attached to the GO samples resulting in the linear increase of the zeta potential of the GO samples.[40,46] These is in well correlation with XRD, Raman and XPS analysis. Hence, increment of the oxidant dosage increases degree of oxidation. As per the American Society for Testing and Materials (ASTM) standards, the zeta potential value for colloidal suspension ranging between 30 and 40 mV shows moderate stability. However, any value higher +40 mV or lower than -40 mV exhibits high stability.[40] Hence, samples GO-1 to GO-5 show high stability in the form of aqueous suspension. Further, this negatively charged behavior of GO is related to both, the pseudocapacitive nature of electrode materials in supercapacitors[46] and for the adsorption of metal ions on GO surface.
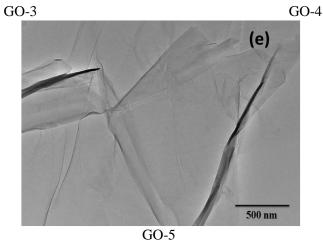
4.6. Morphological studies

The morphological changes due to the degree of oxidation in five GO samples were analyzed by TEM. Fig. 5 shows difference in the transparency of GO sheet, this may due to different number of GO sheet stacked in the structure. The GO-1 shows opaque or less transparent sheet as compare to rest of the GO samples, this may be due to multilayer of partially unoxidized GO sheet. As explained earlier by XRD, Raman and XPS, the percentage of functional group attached to GO sheet in GO-1 sample is minimum, which further restrict the exfoliation of multilayer GO sheet. As the oxidation increases more transparent, thin few layer GO sheets were observed indicating improvement in exfoliation of multilayer sheets, due to

16

1 increment in oxygenated functional groups attached to the GO planes. This is well in co-

2 ordination with information obtained from XRD, XPS and Raman spectroscopy. [19]

3

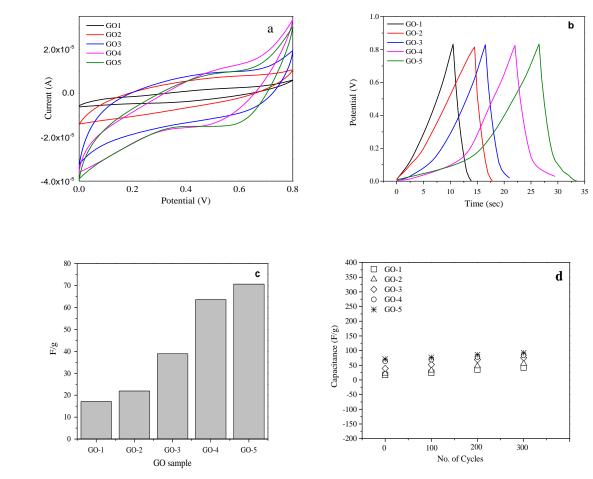**Fig. 5** TEM image of GO-1, GO-2, GO-3, GO-4 and GO-5 samples.

4.7 Electrochemical studies

The cyclic voltammetry of GO in Fig. 6a shows an elliptical curve, deviated from an ideal rectangular voltamogram indicating a faradaic reaction of electrolyte ions at the interface of the electrodes.[47] This charge storage mechanism is a characteristic behavior of pseudocapacitors. The specific capacitance of GO samples were measured by galvanostatic charge/discharge curve shown in Fig. 6b. The charge-discharge curve was obtained at the constant current of 1 A/g and charge storage was calculated to be 17, 21, 36, 64 and 71 F/g for GO-1, GO-2, GO-3, GO-4 and GO-5 respectively (Fig. 6c). The increase in percentage of oxygenated functional group from GO-1 to GO-5 significantly increases the pseudo-capacitance. The presence of functional groups, defects and grain boundaries on the GO planes acts as effective redox centers for the charge storage reactions, due to weak interaction of electrolyte ions with the electrode interface.[48] Enhancement in the charge storage was obtained with the cycles as shown in Fig.6d. This enhancement is due to the better percolation of the electrolyte ions in the electrode material used, with increase in the number of cycles.[49]

The impedance spectra is a direct evidence to understand the behavior of material in actual operating conditions.[32,49] Fig. S5 of ESI shows the electrochemical impedance spectroscopy (EIS) data of five GO samples, which were analyzed by using a Nyquist plot containing imaginary (Z") and real component (Z') of the impedance in the frequency range of 20Hz – 20MHz.[32] As seen from the spectra, the degree of oxidation and charge transfer resistance has direct linear co-relation. The diameter of semicircle curve at higher frequency region represents the ESR of the cell, which depends on the characteristic of the electrode material and ionic accessibility into the electrode material.[50] The diameter of semicircle increase with the increase in degree of oxidation which is an indication of the enhanced ESR of the supercapacitor cell.[49] It was also observed that the Warburg curve was missing which is attributed to the short ion

18

1   diffusion path, which facilitate the efficient access of electrolyte ions to the surfaces of the

2   electrodes (Fig S5 of ESI).[51,52] Further detailed analysis and optimization of the degree of

3   oxidation is required for commercial supercapacitor electrodes.

4

5

6   Fig. 6(a) Cyclic voltammetry obtained at the scan rate of 30 mV/s (b) Galvanostatic charge-

7   discharge obtained at the constant current of 1A/g (c) Charge storage capacitance and (d)

8   Stability curves for GO1, GO-2, GO-3, GO-4 and GO-5 samples.

9

4.8. Adsorption of heavy metal ion

As discussed earlier, increase in the degree of oxidation increases the amount of functional groups (O-C=O, C=O, C-O, C-OH, C-O-C etc) on the surface of GO. These functional groups present in GO assist in forming hydrogen bonding with water molecules leading to stable dispersion of carbon based GO. This dispersion further facilitates the adsorption of heavy metals from the aqueous solution.[23,27] Fig. 7 & 8 shows, as the degree of oxidation increases from GO-1 to GO-5, the adsorption of metal ion viz., Cd (II) and Cu (II) on the surface of GO increases.
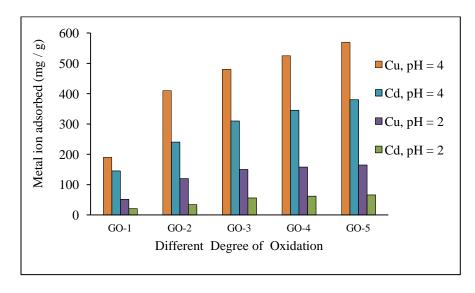
It is well known that with the variation in the pH of the solution, metal ions in water solution may be exist in various forms. For the current study, adsorption of these metal ions was performed at pH = 2 and 4. At pH = 4, more than 90% of Cd is present in its divalent cationic form, while > 99% copper exists as Cu^{2+} ion form.[23] Further, the pH_{pzc} (point of zero charge) value of GO is 3.8–3.9. Therefore, at pH > 3.9 (pH > pH_{pzc}), the electrostatic interactions between the metal ions and GO become stronger or positively charged divalent metal ions undergoes organo-metal ion complexation because the surface charge of GO is negative.[23,27,53] Hence at pH = 4, GO-5 which contains maximum oxygen functionalities shows approximately three times higher adsorption for Cu(II) and 2.5 times higher adsorption for Cd(II) as compared to GO-1. Further, any decrease in the charge on the functional group or metal ion affects the adsorption pattern. . Fig. 7 showed that adsorption of Cu (II) and Cd (II) ion at pH = 2 was less compared to that of pH = 4. This is attributed to the simultaneous presence of high H^+ ions which result in protonation of oxygenated functional groups and also hinder the dissociation of COOH functional groups.[23] At higher pH (pH > 6), Cu (II) and Cd (II) precipitated from the solution, so studies were restricted to pH = 4.

1   The isothermal batch equilibrium adsorption mechanism was understood, by fitting the

2   experimental data into the linear form of with Langmuir isotherm, eqn. (4).[54]

$$q_e = q_{max}.K_L C_e / (1 + K_L C_e) \tag{4}$$

3   where, q_{max} is the maximum metal ion adsorption capacity per unit weight of GO (mg.g^{-1}), C_e is

4   metal ion concentration in aqueous phase at equilibrium (mg.dm^{-3}). K_L represents the Langmuir

5   adsorption constant. The Langmuir adsorption isotherms were obtained by fitting the adsorption

6   equilibrium data to the isotherm model, as shown in Fig. 8 (a & b) for Cu and Cd ions,

7   respectively. The Langmuir model shows the best fit, confirming monolayer adsorption of metal

8   ion on to the surface of GO. It was also observed from the adsorption studies that Cu ions adsorb

9   preferentially compared to Cd(II) ions on the same adsorbent material. This agrees very well

10   with the metal electronegativity values for Cu and Cd. The electronegativity is a contributing

11   parameter in the metal ion uptake by graphene oxide sample.[23,55]

12

13   **Fig.7** Adsorption of cadmium and copper ions on GO with different degree of oxidation at pH 2
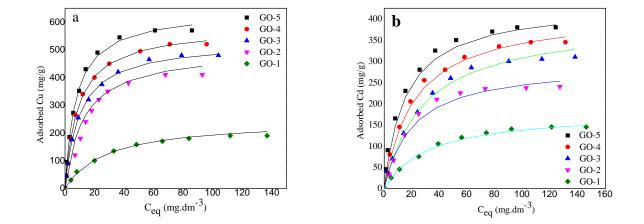
14   & 4.

1 **Fig.8** Adsorption isotherm for (a) copper ions and (b) Cadmium ions on GO with different

2 degree of oxidation at pH = 4.

3 **5. Conclusion**

4   The series of GO with different degree of oxidation have been successfully synthesized

5 by altering the oxidant dose. The XRD, Raman, XPS and zeta potential analysis confirms

6 successive increment in negatively charged oxygenated functional group on the GO surface with

7 increase in oxidation level. As the percentage of oxygenated functional groups present on GO

8 increases, it leads to enhancement in redox pseudocapacitive current, which further boost its

9 charge storage capacity. The negatively charged GO sample exhibits stronger affinity to

10 positively charge metal ion in water. The GO with higher degree of oxidation shows higher

11 adsorption capacity following Langmuir adsorption pattern. The enormous amount of negatively

12 charged functional group on surface of GO, it's good dispersion ability and strong affinity

13 towards metal ion is an important aspect in field of extraction, separation and purification.

14

15 **Acknowledgment**

4   **†Electronic supplementary information (ESI) available**

5   **Fig. S1** Pictorial presentation of the GO samples prepared

6   **Fig. S2** Interlayer spacing for GO samples with different degrees of oxidation.

7   **Fig. S3** Plot I_D / I_G ratio for graphite and different GO samples (GO-1 to GO-5).

8   **Fig. S4** Plot of zeta potential vs. samples with different oxidation levels

9   **Fig. S5**: Impedance *vs* frequency plot of GO1, GO-2, GO-3, GO-4 and GO-5 samples.

10

11

1   **References**

2   1. S.Park and R.S. Ruoff,*Nat. Nanotechnol.*, 2009,**4**(4), 217.

3   2. J. H.Warner, , F. Schaffel, M. Rummeli and A. Bachmatiuk,*Graphene: Fundamentals and*

4   *emergent applications*, Elsevier, Newnes2012, ch. 4.

5   3. D.R. Dreyer, S. Park, C. W. Bielawski and R.S. Ruoff, *Chem. Soc. Rev.,* 2010,**39**(1), 228.

6   4. S.Chen, J. Zhu, X. Wu, Q. Han and X. Wang, *ACS Nano.,* 2010,**4**(5), 2822.

7   5. U.Khan, , P. May, A. O'Neill and J. N. Coleman, *Carbon.,*2010,**48**(14), 4035.

8   6. K.Krishnamoorthy, R. Mohan and S. J. Kim, *Appl. Phys. Lett.,*2011,**98**(24), 244101.

9   7. G.Wang, X. Sun, C. Liu and J. Lian, *Appl. Phys. Lett.,*2011,**99**(5), 053114..

10   8. B.C. Brodie, *Philos. Trans. R. Soc. London,* 1859, **149,** 249.

11   9. W.S. Hummers, Jr., and R. E. Offeman, *J. Am. Chem. Soc.*, 1958, **80**(6), 1339.

12   10. L. Staudenmaier, *Ber. Dtsch. Chem. Ges.*, 1898, **31**, 1481.

13   11. C.Y.Su, Y. Xu, W. Zhang, J. Zhao, A. Liu, X. Tang, C. H. Tsai, Y. Huang and L. J. Li,

14   *Acs. Nano.,*2010,**4**(9), 5285.

15   12. G. Eda, J. Ball, C. Mattevi, M. Acik, L. Artiglia, G. Granozzi, Y. Chabal, T.D.

16   Anthopoulos and M. Chhowalla. *J Mater Chem,* 2011, **21**(30), 11217.

17   13. T. Szabó, O. Berkesi, P. Forgó, K. Josepovits, Y. Sanakis, D. Petridis and I. Dékány,

18   *Chem.Mater.,* 2006, **18**(11), 2740.

1   14. A. Lerf, H. He, M. Forster and J. Klinowski. *J. Phys. Chem. B.*, 1998, **102**(23), 4477.

2   15. N.R. Wilson, P.A. Pandey, R. Beanland, R.J. Young, I.A. Kinloch, L. Gong, Z. Liu, K.

3   Suenaga, J.P. Rourke and S.J. York, *ACS Nano*, 2009, **3**(9), 2547-2556.

4   16. S. Shukla and S. Saxena, *Appl. Phys. Lett.,* 2011, **98**(7), 073104.

5   17. Y. Wang, Z. Shi, Y. Huang, Y. Ma, C. Wang, M. Chen and Y. Chen, *J. Phys. Chem C.*,

6   2009, **113**(30), 13103.

7   18. B. Xu, S. Yue, Z. Sui, X. Zhang, S. Hou, G. Cao and Y. Yang, *Energy Environ. Sci.,* 2011,

8   **4**(8), 2826.

9   19. H. Yan, X. Tao, Z. Yang, K. Li, H. Yang, A. Li and R. Cheng, *J. Hazard. Mater.,* 2014,

10   **268**, 191.

11   20. P. Sharma and M.R. Das., *J. Chem. Eng. Data.*, 2013, **58**(1), 151.

12   21. G. K. Ramesha, A. Vijaya Kumara, H. B. Muralidhara and S. Sampath., *J. Colloid Interf.*

13   *Sci.*, 2011, **361**(1), 270.

14   22. L. Sun, H. Yu and B. Fugetsu, *J. Hazard. Mater.,* 2012, **203– 204**, 101.

15   23. R. Sitko, E. Turek, B. Zawisza, E. Malicka, E. Talik, J. Heimann, A. Gagor, B. Feist, R.

16   Wrzalik., *Dalton Transaction.,* 2013,**42**(16), 5682.

17   24. G. Zhao, J. Li , X. Ren, C. Chen and X. Wang, *Environ. Sci. Tech.*, 2011, **45**(24), 10454.

18   25. F. Zhang, B. Wang, S. He, and R. Man, *J. Chem. Eng. Data.*, 2014, **59**(5)*,* 1719−1726

1   26. Y. Sun, Q. Wang, C. Chen, X. Tan, and X. Wang, *Environ. Sci. Technol.* 2012, **46**(11),

2   6020.

3   27. L. Liu, S. Liu, Q. Zhang, C. Li, C. Bao, X. Liu and P. Xiao, *J. Chem. Eng. Data.* 2013,

4   **58**(2), 209.

5   28. G. Zhao, T. Wen, X. Yang, S. Yang, J. Liao, J. Hu, and X. Wang, *Dalton. Trans.,* 2012,

6   **41**(20), 6182.

7   29. M. Kazemipour, M. Ansari, S. Tajrobehkar, M. Majdzadeh and H. R. Kermani, *J.*

8   *Hazard. Mater.*, 2011, **150**, 322.

9   30. M. Kobya, E. Demirbas, E. Senturk, M. Ince, *Bioresour. Technol.* 2005, **96**, 1518.

10   31. M.M., Kadam, M.B. Sravani, V.G. Gaikar, and N. Jha, *AIP Conf. Proc*., 2013, **1538**, 249.

11   DOI: 10.1063/1.4810067.

12   32. W. Chen, R. B. Rakhi, M. N. Hedhili and H. N. Alshareef, *J. Mater. Chem. A,* 2014, **2**,

13   5236.

14   33. Sheng, Y. Sun, C. Li, W. Yuan and G. Shi, *Scientific Report*, 2012, 2(**247**), 1-5.

15   34. N. A. Kumar, H-J. Choi, Y. R. Shin, D. W. Chang, L. Dai, and J-B. Baek, *ACS Nano,*

16   2012, **6** (2) 1715.

17   35. P. Ramesh, S. Bhagyalakshmi, and S. Sampath *J. Collo. Inter.Sci.,* 2004, **274**, 95.

18   36. D.C. Marcano, D. V. Kosynkin, J. M. Berlin, A. Sinitskii, Z. Sun, A. Slesarev, L. B.

19   Alemany, W. Lu and J. M. Tour, *ACS Nano* 2010, **4**(8), 4806.

20   37. G. Wang, X. Sun, C. Liu and J. Lian, *Appl. Phys. Lett.,* 2011, **99**(5), 053114.

38. G. Venugopal, K. Krishnamoorthy, R. Mohan and S.-J. Kim, *Mater. Chem. Phys.,* 2012, **132**(1), 29.

39. C. Hontoria-Lucas, A. Lopez-Peinado, J. d. D. López-González, M. Rojas-Cervantes and R. Martin-Aranda, *Carbon,* 1995, **33**(11), 1585.

40. K. Krishnamoorthy, M. Veerapandian, K. Yun and S.-J. Kim, *Carbon,* 2013, **53**, 38-49. 39

41. A.C. Ferrari and J. Robertson, *Phys Rev B.,* 2000, **61**, 14095.

42. M.A. Pimenta, G. Dresselhaus, M.S. Dresselhaus, L.G. Cancado, A. Jorioa and R. Saito, *Phys Chem Chem Phys.,* 2007, **9**, 1276.

43. C.H. Lucas, A.J.L. Peinado, D.L. Gonzalez, M.L.R. Cervantes and R.M.M. Aranda, *Carbon*, 1995, **33**, 1585.

44. Y-Li. Huang, H-W. Tien, C-C. M. Ma, S-Y. Yang, S-Y. Wu, H-Y. Liu and Y-W. Mai, *J. Mater. Chem.*, 2011, **21**, 18236.

45. F.A. de La Cruz, and J. Cowley, *Nature,* 1962, **196**, 468.

46. I. Jung, D. A. Dikin, R. D. Piner and R. S. Ruoff, *Nano Lett.*, 2008,**8**(12), 4283.

47. H-K. Jeong, M. Jin, E. J. Ra, K. Y. Sheem, G. H. Han, S. Arepalli, and Y. H. Lee, *ACS Nano*, 2010, **4** (2), 1162.

48. M. Zhi, C. Xiang, J. Li, M. Li and N. Wu, *Nanoscale*, 2013, **5**, 72–88.

49. C. Fu, G. Zhao, H. Zhang and S. Li, *Int. J. Electrochem. Sci.,* **2013, 8**, 6269.

1   50. E. Teer, M. Deraman I. A. Talib, S. A. Hashmi, A. A. Umar, *Electrochim Acta.,* 2011, **56**

2   (27)**,** 10217.

3   51. B. A. Abd-El-Nabey, A. M. Abdel-Gaber, E.Khamis, Aly.I.A. Morgaan1 and N.M.Ali1,

4   *Int. J. Electrochem. Sci.,* 2013, **8**, 11301.

5   52. A. K. Mishra and S. Ramaprabhu, *J. Phys. Chem. C.*, 2011, **115,** 14006.

6   53. S. Park, K-S. Lee, G. Bozoklu, W. Cai, S. T. Nguyen, and R.S. Ruoff, *ACS Nano*, 2008,

7   **2**(3), 572.

8   54. S.T. Yang, Y. Chang, H. Wang, G. Liu, S. Chen, Y. Wang, Y. Liu, A. Cao, *J. Colloid.*

9   *Interf. Sci.,* 2010, **351**(1), 122.

10   55. S.A. Dastgheib and D.A. Rockstraw, *Carbon.*, 2002, **40**(11), 1843.

11